Diffusion of intrinsically disordered proteins within protein condensates

Fuga Watanabe,¹ Takuma Akimoto⁰,² Robert B. Best⁰,³ Kresten Lindorff-Larsen⁰,⁴ Ralf Metzler⁰,^{5,6} and Eiji Yamamoto⁰,*

¹Department of System Design Engineering, Keio University, Yokohama, Kanagawa 223-8522, Japan
²Department of Physics, Tokyo University of Science, Noda, Chiba 278-8510, Japan
³Laboratory of Chemical Physics, National Institute of Diabetes and Digestive and Kidney Diseases,
National Institutes of Health, Bethesda, MD, USA

⁴Linderstrøm-Lang Centre for Protein Science, Department of Biology, University of Copenhagen, DK-2200 Copenhagen N, Denmark

⁵Institute of Physics & Astronomy, University of Potsdam, 14476 Potsdam-Golm, Germany

⁶Asia Pacific Centre for Theoretical Physics, Pohang 37673, Republic of Korea



(Received 14 January 2024; accepted 23 September 2025; published 30 October 2025)

Many intrinsically disordered proteins (IDPs) may undergo a phase separation to form a biomolecular condensate. Understanding the behavior of individual molecules within condensates is crucial for characterizing their collective physical properties relevant to biological functions. Here, we investigate the diffusion dynamics of IDPs within protein condensates using molecular dynamics simulations. We find that the proteins exhibit transient subdiffusion due to the viscoelastic nature of the condensates. Under conditions when confinement arises from the finite size of the droplet, the conformation and instantaneous diffusivity of the proteins vary significantly between the droplet interior and the interface with the environment, resulting in non-Gaussian displacement distributions. Moreover, we demonstrate that the structural complexity and intermolecular interactions of proteins modulate the subdiffusive behavior and the relaxation of diffusivity fluctuations. This study highlights key aspects of the heterogeneous structural and dynamical behavior of IDPs within biomolecular condensates.

DOI: 10.1103/jsdl-chm9

I. INTRODUCTION

Some multivalent proteins and nucleic acids may form biomolecular condensates, also sometimes called membraneless organelles (MLOs), through phase separation [1,2]. Such protein phase separation is often driven by sequence-specific multivalent interactions among the components [3,4]. In addition, entropic effects can influence the formation of protein condensates, particularly in multicomponent systems such as the cellular cytoplasm. There, protein concentrations are high, and depletion interactions and entropic forces can play a significant role [5–7]. Certain intrinsically disordered proteins (IDPs) may, due to their flexibility and specific sequence properties, play a central role in the formation of these condensates [4,8]. The organization of MLOs has been suggested as contributing to essential biological processes, such as gene regulation, biochemical reactions, signal transduction, and molecular protection as a stress response. These functions depend on the unique physical properties of the condensates. The presence of flexible IDPs renders the interior of the condensate highly dynamic and complex, exhibiting liquidlike properties with viscoelasticity [9–14].

Published by the American Physical Society under the terms of the Creative Commons Attribution 4.0 International license. Further distribution of this work must maintain attribution to the author(s) and the published article's title, journal citation, and DOI.

While many studies have examined phase separation and droplet formation of biomolecular condensates, several studies have specifically investigated the dynamics of proteins within condensates using experimental and computational approaches, such as pulsed-field gradient NMR [15–17], fluorescence recovery after photobleaching (FRAP) [18], single-molecule fluorescence microscopy [19–22], and molecular dynamics (MD) simulations [23–28]. The diffusivity of proteins within condensates is typically two to three orders of magnitude lower than in the dilute phase and can be tuned by sequence variation and protein length. It has also been highlighted that the interface of biomolecular condensates acts as a key element in driving pathological protein aggregation [29-31] and that it plays an important role in regulating molecular exchange with the surrounding environment [31,32]. A detailed exploration of the intricate diffusion process of IDPs using physical models could shed light on the properties crucial for cellular processes. However, a comprehensive understanding of the spatiotemporal conformation and dynamics of IDPs within the condensates remains elusive at the molecular scale. In particular, a fundamental understanding of the physics in simpler systems, i.e., composed of a single type of protein, is essential as a benchmark to address the complexities inherent to multicomponent protein condensates.

Here, we perform large-scale MD simulations of protein condensates formed by IDPs to investigate the diffusive dynamics of proteins. We demonstrate that the proteins exhibit transient subdiffusion attributed to anticorrelated motion, which is presumed to be due to the viscoelastic properties

^{*}Contact author: eiji.yamamoto@sd.keio.ac.jp

of the droplet. Furthermore, we show that diffusivity varies between the interior and the interface of the droplets, resulting in a non-Gaussian distribution of displacement.

II. METHODS

A. Molecular dynamics simulations of protein droplets

We performed coarse-grained molecular dynamics (CG-MD) simulations of 1000 molecules of the fused in sarcoma low-complexity domain (FUS-LCD) and N-terminal disordered region of DDX4 (DDX4-DR). The lengths of FUS-LCD and DDX4-DR are 163 and 236 amino acid residues, respectively. We employ FUS-LCD and DDX4-DR as an example of IDP phase separation. FUS is an RNA-binding protein known to be involved in cell function and neurodegenerative diseases [4,33–35]. The sequence-specific interaction of LCD region plays a key role in FUS phase separation, and FUS-LCD can undergo phase separation on its own in vivo and in vitro [4,16,18,35,36]. DDX4 is a major constituent of germ granules and also undergoes phase separation. DDX4 contains an intrinsically disordered N-terminal region and forms membraneless organelles, which are stabilized by electrostatic and cation- π interactions unlike FUS-LCD phase separation [15,37,38].

We adopted the hydropathy scale (HPS) CG model with implicit solvent, a residue-level CG model in which each amino acid is represented by a single bead [39] (see Fig. S9 in the Supplemental Material [40]). We used two parameter sets of the HPS model: the HPS-KR model, which employs a hydrophobicity scale from Kapcha and Rossky [41], and the HPS-Urry model, which utilizes a hydrophobicity scale proposed by Urry et al. [42] and optimized by Regy et al. [43]. The HPS-Urry model is capable of reproducing a sequence-dependent description of phase separation in FUS-LCD and DDX4-DR [43], and was primarily used in the main results of this study. In this model, IDPs are considered as fully flexible polymers. The total potential energy of the HPS model is given by

$$U_{\text{tot}} = U_{\text{Bonds}} + U_{\text{Hydronathy}} + U_{\text{Electrostatic}},$$
 (1)

where $U_{\rm Hydropathy}$ and $U_{\rm Electrostatic}$ represent nonbonded interactions, and $U_{\rm Bonds}$ represents bonded interactions between sequential amino acids. The bonded interactions are described by a harmonic potential,

$$U_{\text{Bonds}} = \sum_{\text{bonds}} k(r - r_0)^2, \tag{2}$$

where the spring constant is $k = 8033 \,\mathrm{kJ} \,\mathrm{mol}^{-1} \,\mathrm{nm}^{-2}$ and the equilibrium bond length is $r_0 = 0.38 \,\mathrm{nm}$.

Nonbonded interactions between amino acids based on their hydropathy are modeled using the Ashbaugh-Hatch potential [44],

$$U_{\text{Hydropathy}} = \sum_{i} \sum_{j < i} \begin{cases} U_{\text{LJ}}(r) + (1 - \lambda_{ij})\epsilon & (r \leqslant 2^{1/6}\sigma_{ij}), \\ \lambda_{ij}U_{\text{LJ}}(r) & (r > 2^{1/6}\sigma_{ij}), \end{cases}$$
(3

where U_{LJ} is the Lennard-Jones potential,

$$U_{\rm LJ} = 4\epsilon \left[\left(\frac{\sigma_{ij}}{r} \right)^{12} - \left(\frac{\sigma_{ij}}{r} \right)^{6} \right],\tag{4}$$

with $\epsilon = 0.8368 \,\mathrm{kJ} \,\mathrm{mol}^{-1}$. The parameters σ_{ij} and λ_{ij} are the arithmetic means of the size and hydropathy values of amino acid residues i and j, respectively. We set a cutoff of 4 nm for the hydropathy interaction.

The electrostatic interactions among charged amino acids are described by the Yukawa (Debye-Hückel) potential,

$$U_{\text{Electrostatic}}(r) = \sum_{i} \sum_{j < i} \frac{q_i q_j e^2}{4\pi \epsilon_0 \epsilon_r r} \exp(-r/D), \quad (5)$$

where q_i and q_j are the charges of amino acids i and j, respectively. Here, ϵ_0 is the vacuum permittivity and ϵ_r is the relative permittivity, which corresponds to the dielectric constant of water. D is the Debye screening length of an electrolyte solution with ionic strength c_s , defined as $D = \sqrt{1/(8\pi B c_s)}$, where B is the Bjerrum length given by $B(\epsilon_r) = e^2/(4\pi \epsilon_0 \epsilon_r k_B T)$. The relative permittivity ϵ_r depends on the simulation temperature T [45],

$$\epsilon_r(T) = \frac{5321}{T} + 233.76 - 0.9297 T + 1.417 \times 10^{-3} T^2 - 8.929 \times 10^{-7} T^3, \quad (6)$$

such that, for example, $\epsilon_r(300 \text{ K}) = 77.7$ and $\epsilon_r(320 \text{ K}) = 70.8$. Electrostatic interactions were truncated and shifted at a cutoff distance of 4 nm. Further details about the potential parameters are provided in Ref. [46].

Simulations were primarily performed at a temperature of $T=300\,\mathrm{K}$. An additional simulation of an FUS-LCD droplet using the HPS-KR model was performed at $T=320\,\mathrm{K}$ to evaluate the temperature dependence (see Fig. S2 in the Supplemental Material [40]). The ionic strength of the solution c_s was set to 150 mM for FUS-LCD [16,18] and 130 mM for DDX4-DR [15,37,38]. The sequences of FUS-LCD and DDX4-DR used in this study correspond to those provided in the supporting information of Regy *et al.* [43].

All simulations were performed using the OpenMM simulation package [47]. Before the long production runs, we performed a slab simulation to facilitate condensate formation. Periodic boundary conditions were applied in all simulations. The initial configuration, consisting of 1000 proteins in fully extended conformations generated using PeptideBuilder [48], was placed in a simulation box with dimensions $l_x = l_y = 15 \, \mathrm{nm}$ and $l_z = 300 \, \mathrm{nm}$. Once a single condensate had formed, it was transferred into a larger cubic simulation box.

The box sizes were 900 nm for the FUS-LCD simulation using the HPS-KR model, 70 nm for the FUS-LCD simulation using the HPS-Urry model, and 80 nm for the DDX4 simulation using the HPS-Urry model. These sizes were significantly larger than the droplet radius (approximately 20 nm), ensuring that a single droplet could exist in isolation and preventing interactions between periodic images. In simulations using the HPS-Urry model, proteins within the condensate occasionally dissociated into the dilute phase. Therefore, relatively small simulation boxes were used to facilitate the return of dissociated proteins to the droplet while still maintaining sufficient separation to avoid interactions between periodic images. After the slab simulation, a 100 ns equilibration run was performed, during which a spherical

droplet formed, followed by a 20 µs production run. Trajectory data were saved every 0.1 ns for analysis.

All systems were simulated under constant volume and temperature conditions using Langevin dynamics with a time step of 10 fs. The Langevin friction coefficient was set to 0.01 ps⁻¹. Trajectories were visualized using VMD software [49]. All simulation scripts used in this study were based on those provided by Tesei *et al.*, available in the supplementary materials of their publication [46].

To quantify the radius of gyration (R_g) of proteins within the droplet, we classified each protein as belonging to either the interior or the interface region based on the distance between its center of mass (COM) and that of the droplet [see Fig. 4(c)]. The boundary between the interior and interface was determined from the radial density profile [see Fig. 4(a)]. Two different definitions have been used to calculate R_g at specific spatial regions: the bin-weighted R_g , which classifies segments based on the positions of individual monomers [50], and the COM-based (unweighted) R_g , which assigns entire chains to spatial regions based on the position of their COM relative to the COM of the condensate [51,52]. These different averaging methods can highlight distinct conformational properties, particularly at the condensate interface [53]. In this work, we used the COM-based R_g .

B. MD simulations of protein condensates without confinement effects

To investigate the diffusion behavior of proteins within large condensates without boundary effects, we performed MD simulations of the dense phase using periodic boundary conditions. To examine how the presence of folded domains and differences in protein size affect diffusion, we simulated three systems: FUS-LCD, full-length FUS (FUS-FULL), and FUS-ΔFold, a variant of FUS-FULL in which the folded domains were replaced with flexible loops. FUS-FULL contains two folded domains: an RNA recognition motif (RRM, residues 285-371) and a zinc finger region (ZF, residues 422-453). The structure of full-length FUS was obtained from AlphaFold predictions, and the conformations of the folded domains were maintained using an elastic network during the simulations. In addition, to correct for the overestimation of interactions involving buried residues in the folded domains, hydropathy-based nonbonded interactions within the folded domains were scaled down by 30% relative to the original HPS parameters [25,26,39]. In FUS- Δ Fold, the folded RRM and ZF domains were replaced with short alanine loops composed of four and five alanines, respectively. This modification preserved the overall R_g of FUS- Δ Fold close to that of FUS-FULL. All simulations were conducted at $T = 300 \,\mathrm{K}$ with 256 protein molecules in each system. The cubic box sizes were set to L = 23.15 nm for FUS-LCD, L = 35.92 nm for FUS-FULL, and $L = 34.30 \,\mathrm{nm}$ for FUS- Δ Fold, chosen to reproduce the average dense-phase density determined from slab simulations (density profiles in slab simulations are shown in Figs. S5B and S8 in the Supplemental Material [40]). These box sizes were reasonably larger than the R_g in the dense phase, to avoid interactions across the periodic boundaries. The total simulation times were 80 us for FUS-LCD, 200 μ s for FUS-FULL, and 40 μ s for FUS- Δ Fold.

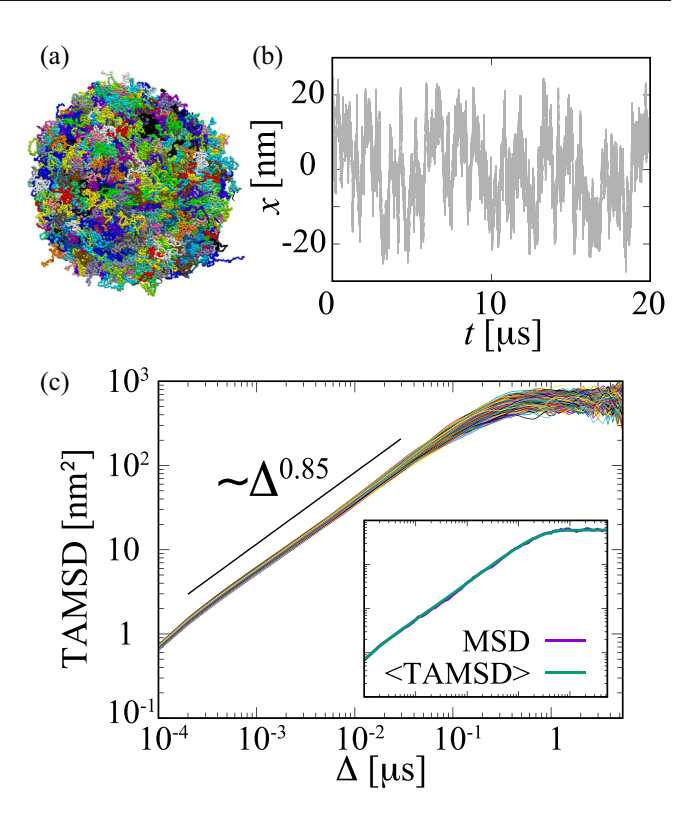


FIG. 1. Diffusion of FUS-LCD within a droplet. (a) Snapshot of the droplet, with a radius of approximately 20 nm, formed by 1000 molecules of FUS-LCD. Each color in the snapshot represents a different protein. (b) Relative x coordinate of a protein with respect to the droplet's COM. (c) TAMSDs for the FUS-LCD proteins within the droplet, where different colors represent different proteins. The inset shows the ensemble-averaged TAMSD and ensemble-averaged MSD.

III. RESULTS

A. Subdiffusive motion of proteins within the droplet

We performed CG-MD simulations of a spherical droplet formed by 1000 copies of a single IDP, the well-studied FUS-LCD, using a residue-level CG model [39,43,46] for 20 μ s [see Fig. 1(a) and Sec. II]. During the simulations, proteins diffuse between the interior and the interface of the droplet several times [Fig. 1(b)]. To characterize the diffusive dynamics of proteins, we calculated the time-averaged mean squared displacement (TAMSD) of the proteins,

$$\overline{\delta_i^2(\Delta;t)} = \frac{1}{t-\Delta} \int_0^{t-\Delta} {\{\mathbf{r}_i(t'+\Delta) - \mathbf{r}_i(t')\}^2 dt'}, \quad (7)$$

where t is the measurement time, Δ is the lag time, and \mathbf{r}_i is the relative coordinate of the COM of the ith protein obtained by subtracting the COM position of the droplet. In what follows, we exclusively analyzed proteins that reside within the droplet during the measurement time. Figure 1(c) shows that TAMSDs of each protein exhibit a sublinear increase, $\delta_i^2(\Delta;t) \propto \Delta^{\alpha}$. The ensemble-averaged TAMSDs indicate $\alpha \approx 0.85$ within the droplets. The amplitude spread of the individual TAMSDs is quite small, consistent with observations of viscoelastic subdiffusion [54,55]. After 1 μ s, the TAMSDs show a plateau, indicative of the spatial confinement

of proteins within the droplet, where the plateau value of the TAMSDs corresponds to the square of the droplet radius, approximately 20 nm. Note that the ensemble-averaged MSD is consistent with the ensemble-averaged TAMSD, indicating that the diffusion process is ergodic [see Fig. 1(c)]. The subdiffusive behavior is distinct from the Brownian motion of an isolated protein in simple liquids, where the ensemble-averaged TAMSD increases linearly. Subdiffusive motion is often observed in molecular diffusion within viscoelastic media, e.g., polymer solutions [56,57] and lipid membranes [54,58–60]. We also found similar subdiffusion for another protein (DDX4) under different temperature conditions and with different model parameters (see Fig. S1 in the Supplemental Material [40]).

B. Anticorrelated motion and non-Gaussian distribution of protein movements

Fractional Brownian motion (FBM) [61,62] and generalized Langevin equations [63,64] are fundamental models of anomalous diffusion characterized by a stochastic motion driven by long-range correlated noise describing the viscoelastic forces acting on the tracer. If the noise exhibits anticorrelation, the TAMSD shows a sublinear increase [55]. Figure 2(a) shows the normalized form of the displacement autocorrelation function (DAF) of proteins,

$$\frac{C_{\Delta}(t)}{C_{\Delta}(0)} = \frac{\langle (\mathbf{r}(t+\Delta) - \mathbf{r}(t))(\mathbf{r}(\Delta) - \mathbf{r}(0))\rangle}{\langle (\mathbf{r}(\Delta) - \mathbf{r}(0))^2 \rangle}, \quad (8)$$

where $\langle \cdot \rangle$ indicates an ensemble average. The transition of the DAF from positive to negative values indicates anticorrelated motion, meaning that, on average, the direction of motion in the next step is likely opposite to that in the preceding step. Such behavior arises naturally in viscoelastic media, where elastic stresses tend to restore particles toward their previous positions [65,66]. The function has a dip at $t=\Delta$, which reflects the degree of anticorrelation, and decays toward zero for long t. Viscoelastic effects are significant on short timescales around $\Delta=10^{-3}\,\mu s$ and gradually diminish over $\Delta=10^{-2}\,\mu s$. Conversely, for longer lag times such as $\Delta=10^{-1}$ and 1 μs , the dip at $t=\Delta$ becomes more pronounced.

In the case of simple FBM, this dip in the DAF at long Δ disappears as viscoelastic effects diminish [67,68]. As discussed further below, using the simulations of protein diffusion in the condensate without confinement effect, we confirmed that the dip in the DAFs with a longer lag time Δ vanishes with a finite correlation time of approximately $\Delta = 10^{-1} \, \mu s$ [Fig. 5(c)]. This timescale is consistent with the crossover time of the MSD from sublinear to linear increase [Fig. 5(a)]. The confinement effect prevents the complete disappearance of the anticorrelation observed in simple FBM; i.e., the anticorrelation at short Δ is due to viscoelastic effects, while that at long Δ results from confinement [67]. Moreover, the confinement effects are more pronounced at $\Delta = 1 \, \mu s$ with a sharp dip to -0.5 [68], where the TAMSDs reach a plateau [Fig. 2(a)].

The normalized DAF exhibits a power-law decay, although it slightly deviates from the simple FBM [67], $C_{\underline{\Delta}}(t)/C_{\underline{\Delta}}(0) \propto t^{\alpha-2}$, where α is the same exponent as in $\delta_i^2(\Delta;t) \propto \Delta^{\alpha}$ [Fig. 2(a)]. As expected from the FBM with a DAF exponent

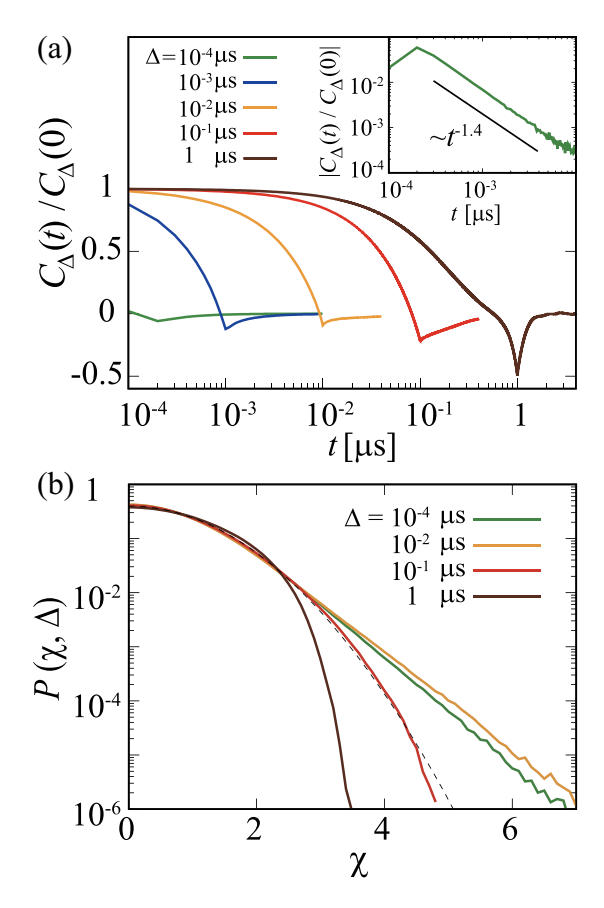


FIG. 2. Anticorrelated motion at short times and non-Gaussianity of FUS-LCD movements within a droplet. (a) Normalized DAFs of the protein with different lag times Δ . The inset shows the log-log plot for $\Delta=10^{-4}\,\mu s$. The black line indicates the theoretical slope of FBM given the measured exponent $\alpha=0.85$. (b) PDFs of the normalized displacement $\chi\equiv |\delta r|/\sigma(\Delta)$ for different lag times Δ , where δr is the displacement in x, y, or z direction and $\sigma(\Delta)$ is the standard deviation of the corresponding displacement distribution for that Δ . All increments from x, y, and z directions are combined into a single set of χ values. The black dashed line represents a Gaussian distribution with unit variance.

of -1.4, the MSD should increase sublinearly with $\alpha = 0.6$. This value is smaller than the TAMSD exponent of $\alpha \approx 0.85$ obtained from Fig. 1(c).

In the case of a simple FBM, the normalized propagator is expected to be Gaussian and consistent for different Δ [55]. To examine the Gaussianity of the displacement, we calculated the propagator $P(\chi, \Delta)$, which represents the probability density function (PDF) of the normalized displacement. Here, χ is defined as the absolute value of the displacement divided by its standard deviation for a given Δ , i.e., $\chi \equiv |\delta r|/\sigma(\Delta)$ with $\delta r \in \{\delta x, \delta y, \delta z\}$, where $\delta x =$ $x(t + \Delta) - x(t)$, and similarly for δy and δz . The quantity $\sigma(\Delta)$ is the standard deviation of the corresponding PDF for lag time Δ . Since no systematic differences were observed in x, y, and z directions, all increments from these directions were combined into a single set of χ values. Figure 2(b) shows that the PDFs of χ for proteins in the droplet exhibit a significantly non-Gaussian profile with exponential tails. On a short timescale, up to $\Delta = 0.1 \,\mu s$, there are significant deviations from the Gaussian distribution in the tails of the PDFs. Such non-Gaussianity has been observed in the diffusion process with fluctuating diffusivity [69–73]; i.e., individual proteins within the droplet diffuse nonuniformly. Conversely, on a long timescale, at $\Delta=0.1\,\mu s$, the PDF is close to the Gaussian distribution. $\Delta=0.1\,\mu s$ is the same timescale at which the TAMSD converges to a plateau [see Fig. 1(c)], which again indicates the confinement effect in the droplet. Due to the confinement effect for longer timescales, e.g., at $\Delta=1\,\mu s$, the propagator exhibits a narrower distribution deviating from the Gaussian distribution for larger displacements χ .

Taken together, both the mismatch between the exponents derived from the DAF ($\alpha \approx 0.6$) and the TAMSD ($\alpha \approx 0.85$) and the observed non-Gaussian propagators with exponential tails demonstrate that the dynamics of proteins in the droplet cannot be fully described by a simple FBM. In fact, stochastic models combining viscoelasticity with heterogeneity in either the diffusivity or the anomalous diffusion exponent have recently been studied and applied to experiments [74–78].

C. Fluctuating diffusivity of proteins within the droplet

As mentioned in the previous section, the non-Gaussian propagators with exponential tails indicate a heterogeneous diffusivity among proteins; i.e., they reflect a fluctuating diffusivity. To quantify the fluctuations, we calculated the relative standard deviation (RSD) of TAMSD [79,80], the square root of the ergodicity breaking parameter [67],

$$RSD = \frac{\sqrt{\langle \delta^2(\Delta;t)}^2 \rangle - \langle \delta^2(\Delta;t) \rangle^2}}{\langle \delta^2(\Delta;t) \rangle}.$$
 (9)

The RSD quantifies the magnitude of variability in diffusivity among different trajectories. In diffusion following a Gaussian process such as Brownian motion, the RSD decays as $t^{-0.5}$, but for nonergodic processes such as continuous-time random walk (CTRW) [55,81] or with significant fluctuation in the diffusivity [82–84], the RSD does not decay to zero even if observed for a long time. In polymeric solutions, the RSD changes from non-Gaussian fluctuations [RSD decays at $t^{-\alpha}(0 < \alpha < 0.5)$] to Gaussian fluctuations (RSD decays at $t^{-0.5}$) because of polymer entanglement, and the crossover time corresponds to the longest relaxation time [79,85]. The RSD of FUS-LCD exhibits a slow decay at short timescales below $t = 0.1 \,\mu\text{s}$, and then a crossover to Gaussian fluctuations (see Fig. 3).

D. Protein conformation and diffusivity inside and in the interface region of droplets

Previous work has shown different conformations of IDPs inside and on the surface of condensates [50–52,86,87]. From the radial number density profile, we define the boundary between the interior and the interface of the droplet at 20 nm, corresponding to the distance from the droplet center where the density starts to decrease toward the interface [see Fig. 4(a)]. We classified each protein as belonging to the interior or interface region based on the distance between its COM and that of the droplet. The PDFs of residence time for the interior and the interface of the droplet exhibit

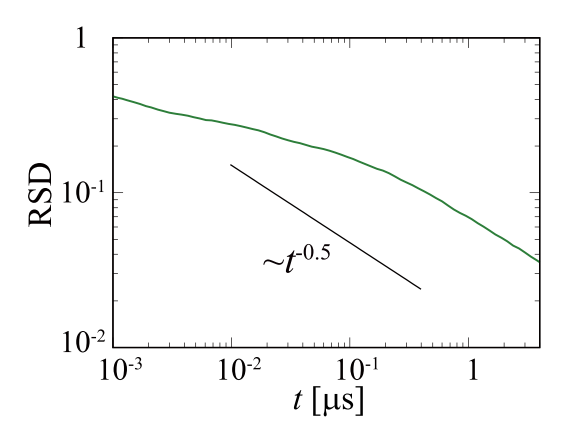


FIG. 3. RSD of FUS-LCD TAMSDs within a droplet. The black solid line is a $t^{-0.5}$ scaling, shown for reference. The RSD was calculated at a lag time of $\Delta = 10^{-4} \, \mu s$.

a power-law distribution with an exponential cutoff $P(t) \propto t^{-\beta} \exp(-t/\tau)$ [see Fig. 4(b)]. The power-law exponent $\beta = -1.5$ is consistent with the first-passage time distribution of one-dimensional Brownian motion [88,89]. The cutoff of the residence time of protein within the droplet interior ($\sim 0.2 \, \mu s$) is comparable to the crossover time of the RSD, suggesting that the non-Gaussian fluctuations are due to transitions between residence in the interior and the interface.

The radius of gyration R_g was calculated from instantaneous configurations of proteins located in each region during the production runs and thus reflects the conformational ensemble in the steady state. The distributions of the radius of gyration R_g exhibit a single peak, with proteins in the interior adopting slightly more expanded conformations than those at the interface [see Fig. 4(c)]. This is consistent with previous simulation studies reporting more compact conformations at the droplet interface [51,52], though we note that different averaging approaches can highlight different conformational properties at the surface [53].

To compare the diffusive dynamics, we calculated the temporary diffusion coefficient (TDC) at time t^* [80,90,91],

$$D(t^*) = \frac{1}{2d\Delta(t-\Delta)} \int_{t^*}^{t^*+t-\Delta} {\{\mathbf{r}(t'+\Delta) - \mathbf{r}(t')\}^2 dt',$$
(10)

where d is the spatial dimension. The lag time Δ can be set to the minimum time step if the time step is longer than the characteristic time of ballistic motion. The measurement time t is a tuning parameter that must be shorter than the characteristic time of the diffusive state [90]. Δ and t were set at 0.1 and 10 ns, respectively. In the TDC analysis, we consider $D(t^*)$ for a protein in the interior or interface regions. The TDC distribution implies that proteins in the interface region diffuse faster than those in the interior of the droplet. This observation is due to the reduced density and smaller size of proteins at the interface compared to those within the droplet [Fig. 4(d)]. The movement between the interior of the droplet and its surface leads to significant fluctuations in diffusivity [Figs. 2(b) and 3]. Note that in this analysis we set d=3 for both regions, as we evaluate the full three-dimensional motion of proteins regardless of their location. If the interface region

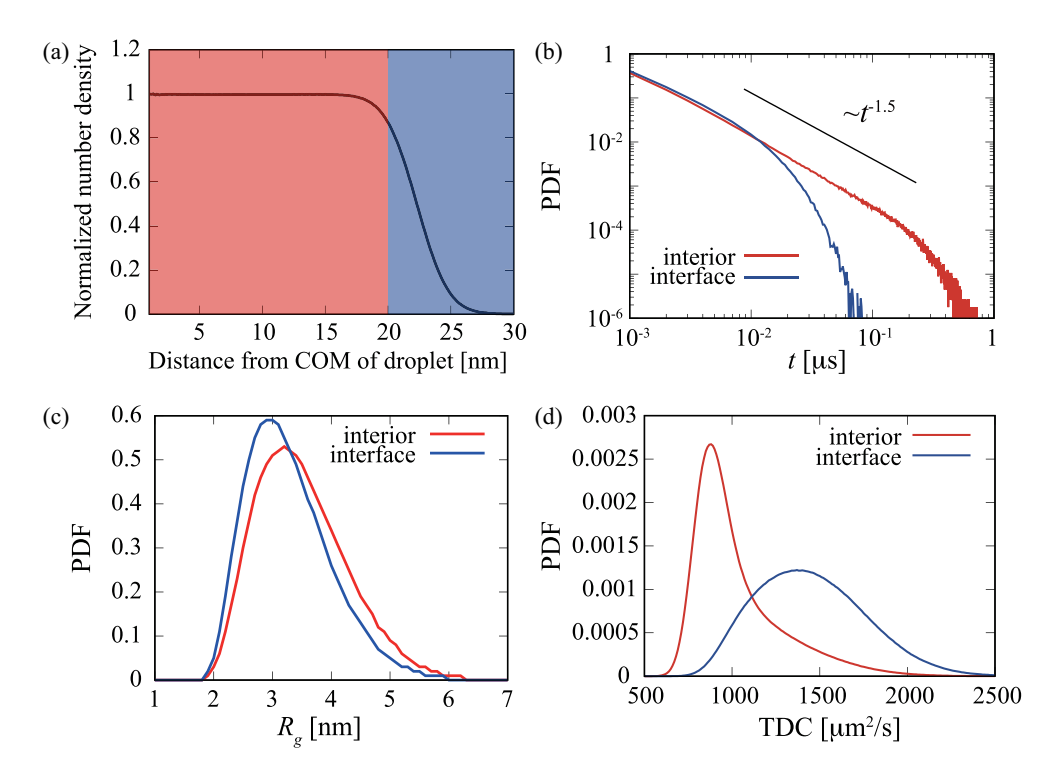


FIG. 4. Difference in conformation and diffusivity of FUS-LCD in the interior and interface regions of a droplet. (a) Normalized radial number density of proteins within the droplet. The red and blue regions correspond to the interior and the interface of the droplet, respectively. (b) PDF of residence times for proteins at the interior and the interface of the droplet. (c) PDFs of R_{ν} and (d) TDC.

were instead treated as a quasi-two-dimensional layer and d set to 2, the calculated $D(t^*)$ values for the interface would increase by a factor of 3/2, further enhancing the diffusivity difference relative to the interior.

E. Universality of the fluctuating diffusivity in droplets across different IDPs, force fields, and thermal conditions

We examined the universality of diffusive protein behavior within spherical droplets by performing MD simulations under various conditions: at different temperatures (300 and 320 K), for the N-terminal disordered region of a different protein (DDX4-DR), and using different force fields (see Figs. S1-S6 in the Supplemental Material [40]). Qualitatively, no clear differences are observed between FUS-LCD and DDX4-DR. When droplets form from 1000 proteins, the density inside the DDX4-DR droplet is lower than that of the FUS-LCD droplet (see Fig. S5 in the Supplemental Material [40]). Additionally, because the residue length of DDX4-DR is greater than that of FUS-LCD, the droplet size of DDX4-DR becomes larger than that of FUS-LCD. This results in slightly faster diffusivity and a longer relaxation time for the fluctuating diffusivity of DDX4-DR compared to those of FUS-LCD (see Fig. 3, and Figs. S4 and S6 in the Supplemental Material [40]).

F. Protein diffusion within large protein condensates

To eliminate the confinement effect caused by the finite size of the droplet, we analyzed protein diffusion within a condensate without finite-size confinement. This was achieved by performing MD simulations of a protein condensate under periodic boundary conditions (details in Sec. II). For the analysis, protein coordinates were used after subtracting the COM motion of the entire system to remove the effect of its translational motion. As shown in Fig. 5(a), FUS-LCD exhibits transient subdiffusion with the same power-law exponent, $\overline{\delta_i^2(\Delta;t)} \propto \Delta^{0.85}$, at short timescales. At longer timescales, diffusion transitions to normal diffusion, following $\propto \Delta$. Unlike proteins in droplets, where TAMSDs plateau at long timescales due to confinement, proteins in a large condensate without boundaries exhibit unrestricted diffusion.

Figure 5(c) shows that DAFs at short timescales are similar to those observed in the droplet [Fig. 2(a)], indicating that viscoelastic effects appear significant. However, in the unconfined condensate, these effects gradually diminish over the range of $\Delta=10^{-3}$ to 10^{-1} µs, confirming the presence of finite anticorrelated motion [Fig. 5(c)]. This timescale is consistent with the crossover time of the TAMSDs, marking the transition from sublinear to linear diffusion. Similar crossover effects were observed in simulations of lipids in bilayer membranes and described in terms of viscoelastic diffusion with tempered correlations [54,92].

Moreover, the RSD follows a $t^{-0.5}$ decay, demonstrating that the significant diffusivity fluctuations seen in the droplet are not observed in the unconfined condensate [Fig. 5(e)]. This result clarifies that the previously observed fluctuations in diffusivity within the droplet originated from proteins moving between the droplet interior and interface. In contrast, within the large condensate without confinement, proteins experience a homogeneous environment, resulting in constant diffusivity. These findings underscore the critical role of heterogeneity arising from differences between the droplet interior and

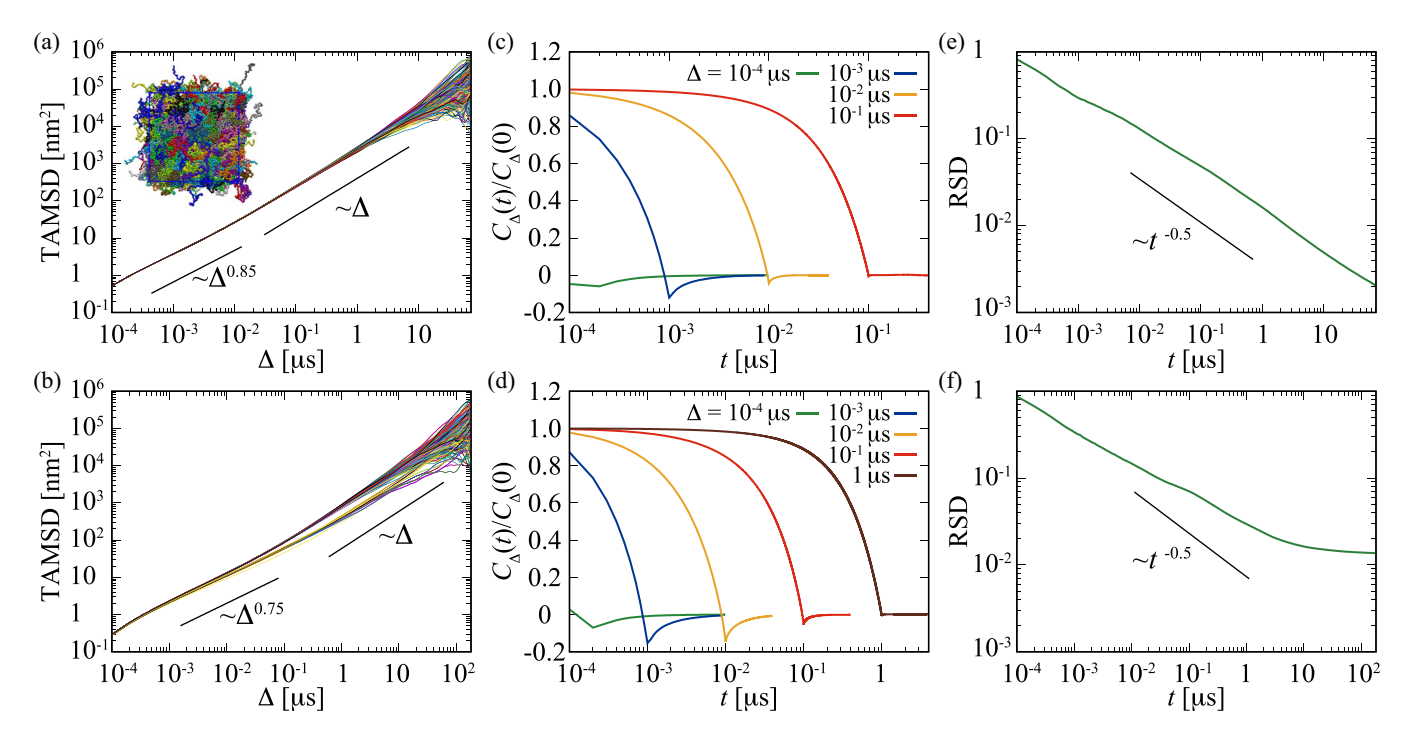


FIG. 5. Diffusion of FUS-LCD and FUS-FULL within large protein condensates. (a) TAMSDs of FUS-LCD. A snapshot of a protein condensate shows a simulation system with periodic boundary conditions modeling protein diffusion within large protein condensates. (b) TAMSDs of FUS-FULL. Normalized DAFs of (c) FUS-LCD and (d) FUS-FULL with different lag times Δ . RSD of TAMSDs for (e) FUS-LCD and (f) FUS-FULL.

interface—in generating fluctuating diffusivity and resulting non-Gaussian behaviors within biomolecular condensates.

G. Influence of the folded domain and protein length on diffusion behavior

IDPs often contain not only disordered regions but also structured (folded) domains, which influence their diffusion behavior. Full-length FUS includes two folded domains: an RNA recognition motif (residues 285–371) and a zinc finger region (residues 422–453). To explore how these domains affect diffusion, we analyzed the behavior of FUS-FULL in an unconfined condensate.

The TAMSDs of FUS-FULL exhibit transient subdiffusion $\delta_i^2(\Delta;t) \propto \Delta^{0.75}$ with a smaller exponent than that of FUS-LCD [Fig. 5(b)]. In addition, the subdiffusive regime is extended to approximately $\Delta=10^{-1}\,\mu s$. This timescale is consistent with the relaxation of the anticorrelated motion, as shown in the DAFs [Fig. 5(d)]. A notable difference is observed in the RSD, which shows a slow decay with a power-law exponent below -0.5 at long measurement times [Fig. 5(f)]; i.e., FUS-FULL exhibits pronounced diffusivity fluctuations compared with FUS-LCD.

Intermolecular contact analysis revealed that the folded RRM and ZF form preferential interactions with intrinsically disordered regions (IDRs) (see Fig. S9 in the Supplemental Material [40]). To eliminate these intermolecular interactions, we replaced the RRM and ZF with alanine loops (referred to as FUS- Δ Fold), consisting of four and five alanines, respectively. Alanine was chosen because it is a small residue without polar or charged side-chain groups, thereby minimizing specific intermolecular interactions, and it is frequently

used in experimental mutagenesis. This modification preserves the R_g of FUS- Δ Fold close to that of FUS-FULL (Fig. S8 in the Supplemental Material [40]). The TAMSD of FUS- Δ Fold exhibits transient subdiffusion with the same exponent as FUS-FULL, but its RSD follows a $t^{-0.5}$ decay (Fig. 6). This result suggests that the long-term fluctuating diffusivity observed in FUS-FULL is attributed to intermolecular interactions between the folded domains and IDRs.

H. Rescaling coarse-grained dynamics to experimental timescales using diffusion coefficients

Performing large-scale MD simulations at the atomic level that are comparable to experimental spatiotemporal scales remains challenging [23]. Residue-level CG-MD simulations with implicit solvent are a unique and powerful tool to explore molecular phenomena over tens to hundreds of nanometers and tens of microseconds [39,93]. However, the diffusion coefficient of proteins within the droplets, as simulated using the CG models, was three orders of magnitude larger than the experimental values [16,18,20]. This implies that simulations of 20 us may correspond to real-time durations of 20 ms (see Fig. S7 in the Supplemental Material [40]). Fast dynamics of the residue-level CG models have also been reported in other studies [25,26], as these models were parameterized to reproduce the structural and phase behavior rather than the dynamic properties [43,93]. The higher diffusivity of residuelevel CG models with implicit solvent is due to the absence of specific interactions between side-chain and backbone atoms, which reduce atomic-scale surface roughness and specific interactions that can slow motion. In addition, although protein condensates contain water molecules and ions, the use of

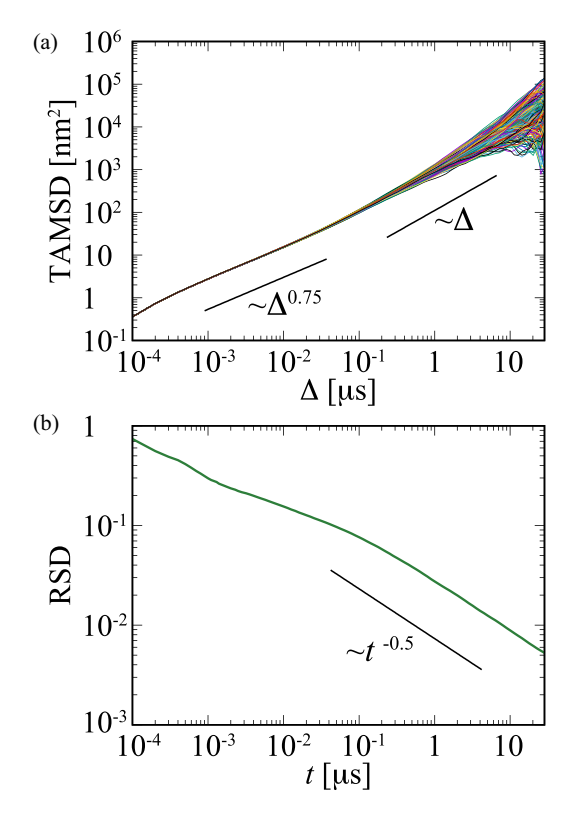


FIG. 6. Diffusion of FUS- Δ Fold within a large protein condensate. (a) TAMSDs and (b) RSD of TAMSDs.

implicit solvent does not capture explicit solvent-mediated friction and short-range hydrodynamic effects within the droplet, thereby further enhancing protein diffusivity in the simulations. One method to match the simulated diffusion coefficients with experimental values is by adjusting the friction coefficient in the Langevin equation. Increasing the friction coefficient by factors of 10–1000 resulted in a decrease of the diffusion coefficient from 200 to $4.0\,\mu\text{m}^2/\text{s}$, respectively, eventually reaching the same order of magnitude as the experimental values. Note that increasing the friction coefficient does not alter the structural property of R_g and the density of the droplets, and the physical mechanism underlying the diffusion process remains qualitatively consistent.

IV. DISCUSSION

In summary, we performed MD simulations to investigate individual protein diffusion within protein condensates. We revealed transient subdiffusion within the condensates caused by anticorrelations in the motion, presumed to be due to their viscoelastic nature. The crossover time corresponds to the relaxation time of anticorrelations. The diffusivity of proteins differs significantly between the interior and the interface region of the droplet. We also demonstrated that the subdiffusion exponent and the magnitude of diffusivity fluctuations depend on the structural complexity and intermolecular interactions, which are influenced by factors such as protein length and the presence of folded domains. This study illustrates that protein diffusion within condensates, characterized by complex amino acid interactions in a crowded environment, follows simple physical models that couple subdiffusion

governed by anticorrelated motion, fluctuation of diffusivity, and confinement effects. Our results provide a molecular interpretation within the framework of diffusion theory [55,76,77,94–96] for macroscopic diffusion phenomena observed in previous experiments. In particular, we show how spatially distinct behaviors between condensate interiors and interfaces emerge from differences in density, conformation, and confinement, thereby clarifying how previously reported interior versus surface conformations of IDPs [50–52,86,87] relate to their molecular dynamics. Furthermore, the modulation of diffusion by the presence or absence of folded domains is comparable to studies showing that internal diffusivity depends on molecular size, interaction strength, and domain composition.

Aging within cellular condensates often changes viscoelastic properties toward a more elastic or even solidlike state [12,14]. This transition is frequently linked to the formation of β -sheet interactions, as well as the nucleation and subsequent growth of amyloidlike structures, which have been observed preferentially at droplet interfaces [29,97]. Such structural ordering generates kinetically hindered regions that confine molecules and reduce molecular diffusivity, potentially leading to ergodicity breaking. A coarse-grained approach incorporating probabilistic transitions to β -sheet formation [29] could reproduce such aging processes, although the observations depend strongly on model parametrization. Our results show that proteins at the droplet interface exhibit lower density, slightly more compact conformations, and faster diffusivity than those in the interior, which could influence where such aging-related structural transitions are initiated, as well as the exchange between the condensate interior and dilute phase.

The observed subdiffusion, characterized by a decreasing effective diffusivity over time, may modulate enzymatic activity and molecular interaction rates [98,99]. For example, enzymatic rates within condensates depend on both their composition and size, with the rate enhancement being larger in smaller droplets [99]. Differences in diffusivity, density, and structure between the droplet interior and interface could give rise to site-dependent interaction propensities, potentially influencing localized condensation or selective molecular exchange at the surface. Such physical features have been implicated in the regulation of biochemical reactions [1], the protection of biomolecules from degradation and stress-induced damage [1], and the spatiotemporal control of translation through mRNA and ribosome organization [100,101]. Although our simulated droplets are smaller and compositionally simpler than intracellular condensates, the underlying physical mechanisms observed here, such as the interplay between anticorrelated motion, heterogeneous diffusivity, and confinement, may provide useful physical insight into how diffusion contributes to the organization and function of cellular condensates.

For a more comprehensive picture, it is important to investigate how a variety of amino acid differences, including the combination of net charges and hydrophobic/hydrophilic properties, affect protein interactions and conformations, and ultimately their diffusive dynamics. Additionally, exploring molecular dynamics within multicomponent condensates, composed of multiple proteins and/or nucleic acids, is essential. These systems exhibit spatiotemporal heterogeneity

[101–105], where dynamically rearranged domains differing in composition, density, or material properties, such as liquidlike regions and more gellike or solidlike subregions, are formed. In such heterogeneous media, a higher degree of fluctuations in diffusivity is expected, similar to those reported in other cellular contexts, such as intermittent trapping in domains [106], transient interactions with partners [107], and heterogeneous diffusivity arising from local environmental variations [75]. Moreover, the spatial patterns and sizes of such compositional domains, along with differences in domain-specific diffusivities, molecular partitioning preferences, and local concentrations, can significantly influence the observed diffusion dynamics [108,109]. However, before addressing such complex systems, it is necessary to clarify the physics underlying the diffusion phenomena in simpler systems. Without this, the fundamental physics of the phenomena could be obscured by several factors contributing to the mechanism of the anomalous diffusions. The presented study thus establishes a benchmark of the fundamental physical phenomena in protein condensates.

ACKNOWLEDGMENTS

This work was supported by JSPS KAKENHI Grant No. 21H05728 and JST PRESTO Grant No. JPMJPR22EE, Japan. This work used computational resources of the supercomputer Fugaku provided by the RIKEN Center for Computational Science through the HPCI System Research Project (Project ID: hp230327). R.M. thanks the German Science Foundation (DFG, Grant No. ME1535/22-1) for support.

DATA AVAILABILITY

The data are available from the authors upon reasonable request.

- [1] S. F. Banani, H. O. Lee, A. A. Hyman, and M. K. Rosen, Biomolecular condensates: Organizers of cellular biochemistry, Nat. Rev. Mol. Cell Biol. 18, 285 (2017).
- [2] R. V. Pappu, S. R. Cohen, F. Dar, M. Farag, and M. Kar, Phase transitions of associative biomacromolecules, Chem. Rev. 123, 8945 (2023).
- [3] A. A. Hyman, C. A. Weber, and F. Jülicher, Liquid-liquid phase separation in biology, Annu. Rev. Cell Dev. Biol. 30, 39 (2014).
- [4] J. Wang, J.-M. Choi, A. S. Holehouse, H. O. Lee, X. Zhang, M. Jahnel, S. Maharana, R. Lemaitre, A. Pozniakovsky, D. Drechsel, I. Poser, R. V. Pappu, S. Alberti, and A. A. Hyman, A molecular grammar governing the driving forces for phase separation of prion-like RNA binding proteins, Cell 174, 688 (2018)
- [5] C. N. Likos, Effective interactions in soft condensed matter physics, Phys. Rep. 348, 267 (2001).
- [6] A. A. Louis, E. Allahyarov, H. Löwen, and R. Roth, Effective forces in colloidal mixtures: From depletion attraction to accumulation repulsion, Phys. Rev. E 65, 061407 (2002).
- [7] M. Majka and P. F. Góra, Analytical theory of effective interactions in binary colloidal systems of soft particles, Phys. Rev. E 90, 032303 (2014).
- [8] D. S. W. Protter, B. S. Rao, B. Van Treeck, Y. Lin, L. Mizoue, M. K. Rosen, and R. Parker, Intrinsically disordered regions can contribute promiscuous interactions to RNP granule assembly, Cell Rep. 22, 1401 (2018).
- [9] C. P. Brangwynne, C. R. Eckmann, D. S. Courson, A. Rybarska, C. Hoege, J. Gharakhani, F. Jülicher, and A. A. Hyman, Germline P granules are liquid droplets that localize by controlled dissolution/condensation, Science 324, 1729 (2009).
- [10] S. Elbaum-Garfinkle, Y. Kim, K. Szczepaniak, C. C.-H. Chen, C. R. Eckmann, S. Myong, and C. P. Brangwynne, The disordered P granule protein LAF-1 drives phase separation into droplets with tunable viscosity and dynamics, Proc. Natl. Acad. Sci. USA 112, 7189 (2015).
- [11] L. M. Jawerth, M. Ijavi, M. Ruer, S. Saha, M. Jahnel, A. A. Hyman, F. Jülicher, and E. Fischer-Friedrich, Salt-dependent

- rheology and surface tension of protein condensates using optical traps, Phys. Rev. Lett. **121**, 258101 (2018).
- [12] L. Jawerth, E. Fischer-Friedrich, S. Saha, J. Wang, T. Franzmann, X. Zhang, J. Sachweh, M. Ruer, M. Ijavi, S. Saha, J. Mahamid, A. A. Hyman, and F. Jülicher, Protein condensates as aging Maxwell fluids, Science 370, 1317 (2020).
- [13] I. Alshareedah, M. M. Moosa, M. Pham, D. A. Potoyan, and P. R. Banerjee, Programmable viscoelasticity in protein-RNA condensates with disordered sticker-spacer polypeptides, Nat. Commun. 12, 6620 (2021).
- [14] I. Alshareedah, W. M. Borcherds, S. R. Cohen, A. Singh, A. E. Posey, M. Farag, A. Bremer, G. W. Strout, D. T. Tomares, R. V. Pappu, T. Mittag, and P. R. Banerjee, Sequence-specific interactions determine viscoelasticity and ageing dynamics of protein condensates, Nat. Phys. 20, 1482 (2024).
- [15] J. P. Brady, P. J. Farber, A. Sekhar, Y.-H. Lin, R. Huang, A. Bah, T. J. Nott, H. S. Chan, A. J. Baldwin, J. D. Forman-Kay, and L. E. Kay, Structural and hydrodynamic properties of an intrinsically disordered region of a germ cell-specific protein on phase separation, Proc. Natl. Acad. Sci. USA 114, E8194 (2017).
- [16] A. C. Murthy, G. L. Dignon, Y. Kan, G. H. Zerze, S. H. Parekh, J. Mittal, and N. L. Fawzi, Molecular interactions underlying liquid-liquid phase separation of the FUS low-complexity domain, Nat. Struct. Mol. Biol. 26, 637 (2019).
- [17] S. Guseva, V. Schnapka, W. Adamski, D. Maurin, R. W. H. Ruigrok, N. Salvi, and M. Blackledge, Liquid-liquid phase separation modifies the dynamic properties of intrinsically disordered proteins, J. Am. Chem. Soc. 145, 10548 (2023).
- [18] K. A. Burke, A. M. Janke, C. L. Rhine, and N. L. Fawzi, Residue-by-residue view of *in vitro* FUS granules that bind the C-terminal domain of RNA polymerase II, Mol. Cell **60**, 231 (2015).
- [19] R. S. Fisher and S. Elbaum-Garfinkle, Tunable multiphase dynamics of arginine and lysine liquid condensates, Nat. Commun. 11, 4628 (2020).
- [20] K. Kamagata, N. Iwaki, M. K. Hazra, S. Kanbayashi, T. Banerjee, R. Chiba, S. Sakomoto, V. Gaudon, B. Castaing, H. Takahashi, M. Kimura, H. Oikawa, S. Takahashi, and

- Y. Levy, Molecular principles of recruitment and dynamics of guest proteins in liquid droplets, Sci. Rep. 11, 19323 (2021).
- [21] K. Kamagata, N. Iwaki, S. Kanbayashi, T. Banerjee, R. Chiba, V. Gaudon, B. Castaing, and S. Sakomoto, Structure-dependent recruitment and diffusion of guest proteins in liquid droplets of FUS, Sci. Rep. 12, 7101 (2022).
- [22] G. Muñoz-Gil, C. Romero-Aristizabal, N. Mateos, F. Campelo, L. I de Llobet Cucalon, M. Beato, M. Lewenstein, M. F. Garcia-Parajo, and J. A. Torreno-Pina, Stochastic particle unbinding modulates growth dynamics and size of transcription factor condensates in living cells, Proc. Natl. Acad. Sci. USA 119, e2200667119 (2022).
- [23] W. Zheng, G. L. Dignon, N. Jovic, X. Xu, R. M. Regy, N. L. Fawzi, Y. C. Kim, R. B. Best, and J. Mittal, Molecular details of protein condensates probed by microsecond long atomistic simulations, J. Phys. Chem. B 124, 11671 (2020).
- [24] Z. Benayad, S. von Bülow, L. S. Stelzl, and G. Hummer, Simulation of FUS protein condensates with an adapted coarse-grained model, J. Chem. Theory Comput. 17, 525 (2021).
- [25] A. R. Tejedor, A. Garaizar, J. Ramírez, and J. R. Espinosa, RNA modulation of transport properties and stability in phaseseparated condensates, Biophys. J. 120, 5169 (2021).
- [26] A. R. Tejedor, I. Sanchez-Burgos, M. Estevez-Espinosa, A. Garaizar, R. Collepardo-Guevara, J. Ramirez, and J. R. Espinosa, Protein structural transitions critically transform the network connectivity and viscoelasticity of RNA-binding protein condensates but RNA can prevent it, Nat. Commun. 13, 5717 (2022).
- [27] S. Ranganathan and E. Shakhnovich, The physics of liquid-to-solid transitions in multi-domain protein condensates, Biophys. J. **121**, 2751 (2022).
- [28] N. Galvanetto, M. T. Ivanović, A. Chowdhury, A. Sottini, M. F. Nüesch, D. Nettels, R. B. Best, and B. Schuler, Extreme dynamics in a biomolecular condensate, Nature (London) 619, 876 (2023).
- [29] Y. Shen, A. Chen, W. Wang, F. S. Ruggeri, S. Aime, Z. Wang, S. Qamar, J. R. Espinosa, A. Garaizar, R. Collepardo-Guevara, D. A. Weitz, D. Vigolo, and T. P. J. Knowles, The liquid-to-solid transition of FUS is promoted by the condensate surface. Proc. Natl. Acad. Sci. USA 120, e2301366120 (2023).
- [30] M. Linsenmeier, L. Faltova, C. Morelli, U. Capasso Palmiero, C. Seiffert, A. M. Küffner, D. Pinotsi, J. Zhou, R. Mezzenga, and P. Arosio, The interface of condensates of the hnRNPA1 low-complexity domain promotes formation of amyloid fibrils, Nat. Chem. 15, 1340 (2023).
- [31] T. Das, F. K. Zaidi, M. Farag, K. M. Ruff, T. S. Mahendran, A. Singh, X. Gui, J. Messing, J. P. Taylor, P. R. Banerjee, R. V. Pappu, and T. Mittag, Tunable metastability of condensates reconciles their dual roles in amyloid fibril formation, Mol. Cell 85, 2230 (2025).
- [32] S. Bo, L. Hubatsch, J. Bauermann, C. A. Weber, and F. Jülicher, Stochastic dynamics of single molecules across phase boundaries, Phys. Rev. Res. 3, 043150 (2021).
- [33] Z. Sun, Z. Diaz, X. Fang, M. P. Hart, A. Chesi, J. Shorter, and A. D. Gitler, Molecular determinants and genetic modifiers of aggregation and toxicity for the ALS disease protein FUS/TLS, PLoS Biol. 9, e1000614 (2011).
- [34] A. Patel, H. O. Lee, L. Jawerth, S. Maharana, M. Jahnel, M. Y. Hein, S. Stoynov, J. Mahamid, S. Saha, T. M. Franzmann, A.

- Pozniakovski, I. Poser, N. Maghelli, L. A. Royer, M. Weigert, E. W. Myers, S. Grill, D. Drechsel, A. A. Hyman, and S. Alberti, A liquid-to-solid phase transition of the ALS protein FUS accelerated by disease mutation, Cell **162**, 1066 (2015).
- [35] S. Qamar, GuoZhen Wang, S. J. Randle, F. S. Ruggeri, J. A. Varela, J. Q. Lin, E. C. Phillips, A. Miyashita, D. Williams, F. Ströhl *et al.*, FUS phase separation is modulated by a molecular chaperone and methylation of arginine cation- π interactions, Cell **173**, 720 (2018).
- [36] T. Murakami, S. Qamar, J. Q. Lin, G. S. K. Schierle, E. Rees, A. Miyashita, A. R. Costa, R. B. Dodd, F. T. S. Chan, C. H. Michel *et al.*, ALS/FTD mutation-induced phase transition of FUS liquid droplets and reversible hydrogels into irreversible hydrogels impairs RNP granule function, Neuron 88, 678 (2015).
- [37] T. J. Nott, E. Petsalaki, P. Farber, D. Jervis, E. Fussner, A. Plochowietz, T. D. Craggs, D. P. Bazett-Jones, T. Pawson, J. D. Forman-Kay, and A. J. Baldwin, Phase transition of a disordered nuage protein generates environmentally responsive membraneless organelles, Mol. Cell 57, 936 (2015).
- [38] R. M. Vernon, P. A. Chong, B. Tsang, T. H. Kim, A. Bah, P. Farber, H. Lin, and J. D. Forman-Kay, Pi-Pi contacts are an overlooked protein feature relevant to phase separation, eLife 7, e31486 (2018).
- [39] G. L. Dignon, W. Zheng, Y. C. Kim, R. B Best, and J. Mittal, Sequence determinants of protein phase behavior from a coarse-grained model, PLoS Comput. Biol. 14, e1005941 (2018).
- [40] See Supplemental Material at http://link.aps.org/supplemental/ 10.1103/jsdl-chm9 for Figs. S1-S9, including universality across proteins, temperatures, and force fields, time rescaling to match simulated diffusion coefficients to experiments, and contact map analysis.
- [41] L. H. Kapcha and P. J. Rossky, A simple atomic-level hydrophobicity scale reveals protein interfacial structure, J. Mol. Biol. **426**, 484 (2014).
- [42] D. W. Urry, D. C. Gowda, T. M. Parker, C.-H. Luan, M. C. Reid, C. M. Harris, A. Pattanaik, and R. D. Harris, Hydrophobicity scale for proteins based on inverse temperature transitions, Biopolymers 32, 1243 (1992).
- [43] R. M. Regy, J. Thompson, Y. C. Kim, and J. Mittal, Improved coarse-grained model for studying sequence dependent phase separation of disordered proteins, Protein Sci. 30, 1371 (2021).
- [44] H. S. Ashbaugh and H. W. Hatch, Natively unfolded protein stability as a coil-to-globule transition in charge/hydropathy space, J. Am. Chem. Soc. **130**, 9536 (2008).
- [45] G. C. Akerlof and H. I. Oshry, The dielectric constant of water at high temperatures and in equilibrium with its vapor, J. Am. Chem. Soc. 72, 2844 (1950).
- [46] G. Tesei, T. K. Schulze, R. Crehuet, and K. Lindorff-Larsen, Accurate model of liquid-liquid phase behavior of intrinsically disordered proteins from optimization of single-chain properties, Proc. Natl. Acad. Sci. USA 118, e2111696118 (2021).
- [47] P. Eastman, J. Swails, J. D. Chodera, R. T. McGibbon, Y. Zhao, K. A. Beauchamp, L.-P. Wang, A. C. Simmonett, M. P. Harrigan, C. D. Stern *et al.*, OpenMM 7: Rapid development of high performance algorithms for molecular dynamics, PLoS Comput. Biol. 13, e1005659 (2017).

- [48] M. Z. Tien, D. K. Sydykova, A. G. Meyer, and C. O. Wilke, PeptideBuilder: A simple Python library to generate model peptides, PeerJ 1, e80 (2013).
- [49] W. Humphrey, A. Dalke, and K. Schulten, VMD: Visual molecular dynamics, J. Mol. Graphics 14, 33 (1996).
- [50] M. Farag, S. R. Cohen, W. M. Borcherds, A. Bremer, T. Mittag, and R. V. Pappu, Condensates formed by prion-like low-complexity domains have small-world network structures and interfaces defined by expanded conformations, Nat. Commun. 13, 7722 (2022).
- [51] J. Wang, D. S. Devarajan, A. Nikoubashman, and J. Mittal, Conformational properties of polymers at droplet interfaces as model systems for disordered proteins, ACS Macro Lett. 12, 1472 (2023).
- [52] D. J. Bauer and A. Nikoubashman, The conformations of protein chains at the interface of biomolecular condensates, Nat. Commun. 15, 9975 (2024).
- [53] G. Chauhan, M. Farag, S. R. Cohen, and R. V. Pappu, Reply to: The conformations of protein chains at the interface of biomolecular condensates, Nat. Commun. 15, 9974 (2024).
- [54] J.-H. Jeon, H. M.-S. Monne, M. Javanainen, and R. Metzler, Anomalous diffusion of phospholipids and cholesterols in a lipid bilayer and its origins, Phys. Rev. Lett. 109, 188103 (2012).
- [55] R. Metzler, J.-H. Jeon, A. G. Cherstvy, and E. Barkai, Anomalous diffusion models and their properties: non-stationarity, non-ergodicity, and ageing at the centenary of single particle tracking, Phys. Chem. Chem. Phys. 16, 24128 (2014).
- [56] T. G. Mason and D. A. Weitz, Optical measurements of frequency-dependent linear viscoelastic moduli of complex fluids, Phys. Rev. Lett. 74, 1250 (1995).
- [57] T. G. Mason, K. Ganesan, J. H. van Zanten, D. Wirtz, and S. C. Kuo, Particle tracking microrheology of complex fluids, Phys. Rev. Lett. 79, 3282 (1997).
- [58] T. Akimoto, E. Yamamoto, K. Yasuoka, Y. Hirano, and M. Yasui, Non-Gaussian fluctuations resulting from power-law trapping in a lipid bilayer, Phys. Rev. Lett. 107, 178103 (2011).
- [59] E. Yamamoto, T. Akimoto, M. Yasui, and K. Yasuoka, Origin of subdiffusion of water molecules on cell membrane surfaces, Sci. Rep. 4, 4720 (2014).
- [60] J.-H. Jeon, M. Javanainen, H. Martinez-Seara, R. Metzler, and I. Vattulainen, Protein crowding in lipid bilayers gives rise to non-Gaussian anomalous lateral diffusion of phospholipids and proteins, Phys. Rev. X 6, 021006 (2016).
- [61] A. N. Kolmogorov, The Wiener spiral and some other interesting curves in Hilbert space, Dokl. Acad. Sci. USSR 26, 115 (1940).
- [62] B. B. Mandelbrot and J. W. Van Ness, Fractional Brownian motions, fractional noises and applications, SIAM Rev. 10, 422 (1968).
- [63] R. Kubo, The fluctuation-dissipation theorem, Rep. Prog. Phys. 29, 255 (1966).
- [64] I. Goychuk, Viscoelastic subdiffusion: From anomalous to normal, Phys. Rev. E **80**, 046125 (2009).
- [65] F. Ginot, J. Caspers, L. F. Reinalter, K. K. Kumar, M. Krüger, and C. Bechinger, Recoil experiments determine the eigenmodes of viscoelastic fluids, New J. Phys. 24, 123013 (2022).
- [66] S. S. Vaidya, L. Muruga, J. Caspers, M. Krüger, and C. Bechinger, Observation and control of nonmonotonic recoils in a viscoelastic fluid, Phys. Rev. Res. 7, 033084 (2025).

- [67] S. Burov, J. H. Jeon, R. Metzler, and E. Barkai, Single particle tracking in systems showing anomalous diffusion: The role of weak ergodicity breaking, Phys. Chem. Chem. Phys. 13, 1800 (2011).
- [68] S. C. Weber, M. A. Thompson, W. E. Moerner, A. J. Spakowitz, and J. A. Theriot, Analytical tools to distinguish the effects of localization error, confinement, and medium elasticity on the velocity autocorrelation function, Biophys. J. 102, 2443 (2012).
- [69] B. Wang, J. Kuo, S. C. Bae, and S. Granick, When Brownian diffusion is not Gaussian, Nat. Mater. 11, 481 (2012).
- [70] M. V. Chubynsky and G. W. Slater, Diffusing diffusivity: A model for anomalous, yet Brownian, diffusion, Phys. Rev. Lett. 113, 098302 (2014).
- [71] W. He, H. Song, Y. Su, L. Geng, B. J. Ackerson, H. B. Peng, and P. Tong, Dynamic heterogeneity and non-Gaussian statistics for acetylcholine receptors on live cell membrane, Nat. Commun. 7, 11701 (2016).
- [72] A. G. Cherstvy and R. Metzler, Anomalous diffusion in time-fluctuating diffusivity landscapes: Stationary and nonstationary cases, Phys. Chem. Chem. Phys. 18, 23840 (2016).
- [73] A. V. Chechkin, F. Seno, R. Metzler, and I. M. Sokolov, Brownian yet non-Gaussian diffusion: From superstatistics to subordination of diffusing diffusivities, Phys. Rev. X 7, 021002 (2017).
- [74] A. G. Cherstvy, S. Thapa, C. E. Wagner, and R. Metzler, Non-Gaussian, non-ergodic, and non-Fickian diffusion of tracers in mucin hydrogels, Soft Matter 15, 2526 (2019).
- [75] A. Sabri, X. Xu, D. Krapf, and M. Weiss, Elucidating the origin of heterogeneous anomalous diffusion in the cytoplasm of mammalian cells, Phys. Rev. Lett. 125, 058101 (2020).
- [76] M. Balcerek, A. Wyłomańska, K. Burnecki, R. Metzler, and D. Krapf, Modelling intermittent anomalous diffusion with switching fractional Brownian motion, New J. Phys. 25, 103031 (2023).
- [77] W. Wang, Q. Wei, A. V. Chechkin, and R. Metzler, Different behaviors of diffusing diffusivity dynamics based on three different definitions of fractional Brownian motion, Phys. Rev. E 112, 014108 (2025).
- [78] M. Balcerek, S. Thapa, K. Burnecki, H. Kantz, R. Metzler, A. Wyłomańska, and A. Chechkin, Multifractional Brownian motion with telegraphic, stochastically varying exponent, Phys. Rev. Lett. 134, 197101 (2025).
- [79] T. Uneyama, T. Akimoto, and T. Miyaguchi, Crossover time in relative fluctuations characterizes the longest relaxation time of entangled polymers, J. Chem. Phys. 137, 114903 (2012).
- [80] E. Yamamoto, T. Akimoto, A. C. Kalli, K. Yasuoka, and M. S. P. Sansom, Dynamic interactions between a peripheral membrane protein and lipids induce a fluctuating diffusion coefficient, Sci. Adv. 3, e1601871 (2017).
- [81] Y. He, S. Burov, R. Metzler, and E. Barkai, Random time-scale invariant diffusion and transport coefficients, Phys. Rev. Lett. **101**, 058101 (2008).
- [82] T. Akimoto and E. Yamamoto, Distributional behaviors of time-averaged observables in the Langevin equation with fluctuating diffusivity: Normal diffusion but anomalous fluctuations, Phys. Rev. E 93, 062109 (2016).
- [83] T. Miyaguchi, T. Akimoto, and E. Yamamoto, Langevin equation with fluctuating diffusivity: A two-state model, Phys. Rev. E **94**, 012109 (2016).

- [84] T. Akimoto and E. Yamamoto, Distributional behavior of diffusion coefficients obtained by single trajectories in annealed transit time model, J. Stat. Mech. (2016) 123201.
- [85] T. Uneyama, T. Miyaguchi, and T. Akimoto, Fluctuation analysis of time-averaged mean-square displacement for the Langevin equation with time-dependent and fluctuating diffusivity, Phys. Rev. E 92, 032140 (2015).
- [86] N. A. Erkamp, M. Farag, Y. Qiu, D. Qian, T. Sneideris, T. Wu, T. J. Welsh, H. Ausserwöger, T. J. Krug, G. Chauhan, D. A. Weitz, M. D. Lew, T. P. J. Knowles, and R. V. Pappu, Differential interactions determine anisotropies at interfaces of RNA-based biomolecular condensates, Nat. Commun. 16, 3463 (2025).
- [87] S. von Bülow, G. Tesei, and K. Lindorff-Larsen, Prediction of phase-separation propensities of disordered proteins from sequence, bioRxiv (2024), https://doi.org/10.1101/2024.06.03. 597109.
- [88] I. Karatzas and S. E. Shreve, Brownian Motion and Stochastic Calculus (Springer, New York, NY, 1991), Vol. 113.
- [89] A. Godec and R. Metzler, Universal proximity effect in target search kinetics in the few-encounter limit, Phys. Rev. X 6, 041037 (2016).
- [90] T. Akimoto and E. Yamamoto, Detection of transition times from single-particle-tracking trajectories, Phys. Rev. E 96, 052138 (2017).
- [91] E. Yamamoto, T. Akimoto, A. Mitsutake, and R. Metzler, Universal relation between instantaneous diffusivity and radius of gyration of proteins in aqueous solution, Phys. Rev. Lett. 126, 128101 (2021).
- [92] D. Molina-Garcia, T. Sandev, H. Safdari, G. Pagnini, A. Chechkin, and R. Metzler, Crossover from anomalous to normal diffusion: Truncated power-law noise correlations and applications to dynamics in lipid bilayers, New J. Phys. 20, 103027 (2018).
- [93] J. A. Joseph, A. Reinhardt, A. Aguirre, P. Y. Chew, K. O. Russell, J. R. Espinosa, A. Garaizar, and R. Collepardo-Guevara, Physics-driven coarse-grained model for biomolecular phase separation with near-quantitative accuracy, Nat. Comput. Sci. 1, 732 (2021).
- [94] G. Muñoz-Gil, G. Volpe, M. A. Garcia-March, E. Aghion, A. Argun, C. B. Hong, T. Bland, S. Bo, J. A. Conejero, N. Firbas et al., Objective comparison of methods to decode anomalous diffusion, Nat. Commun. 12, 6253 (2021).
- [95] H. Seckler and R. Metzler, Bayesian deep learning for error estimation in the analysis of anomalous diffusion, Nat. Commun. 13, 6717 (2022).
- [96] T. Miyaguchi, Generalized Langevin equation with fluctuating diffusivity, Phys. Rev. Res. 4, 043062 (2022).

- [97] L. Emmanouilidis, E. Bartalucci, Y. Kan, M. Ijavi, M. E. Pérez, P. Afanasyev, D. Boehringer, J. Zehnder, S. H. Parekh, M. Bonn, T. C. T. Michaels, T. Wiegand, and F. H.-T. Allain, A solid beta-sheet structure is formed at the surface of FUS droplets during aging, Nat. Chem. Biol. 20, 1044 (2024).
- [98] A. Testa, M. Dindo, A. A. Rebane, B. Nasouri, R. W. Style, R. Golestanian, E. R. Dufresne, and P. Laurino, Sustained enzymatic activity and flow in crowded protein droplets, Nat. Commun. 12, 6293 (2021).
- [99] M. Gil-Garcia, A. I. Benítez-Mateos, M. Papp, F. Stoffel, C. Morelli, K. Normak, K. Makasewicz, L. Faltova, F. Paradisi, and P. Arosio, Local environment in biomolecular condensates modulates enzymatic activity across length scales, Nat. Commun. 15, 3322 (2024).
- [100] D. S. W. Protter and R. Parker, Principles and properties of stress granules, Trends Cell Biol. 26, 668 (2016).
- [101] T. Hirose, K. Ninomiya, S. Nakagawa, and T. Yamazaki, A guide to membraneless organelles and their various roles in gene regulation, Nat. Rev. Mol. Cell Biol. 24, 288 (2023).
- [102] C. M. Fare, A. Villani, L. E. Drake, and J. Shorter, Higher-order organization of biomolecular condensates, Open Biol. 11, 210137 (2021).
- [103] D. L. J. Lafontaine, J. A. Riback, R. Bascetin, and C. P. Brangwynne, The nucleolus as a multiphase liquid condensate, Nat. Rev. Mol. Cell Biol. 22, 165 (2021).
- [104] T. Wu, M. R. King, Y. Qiu, M. Farag, R. V. Pappu, and M. D. Lew, Single-fluorogen imaging reveals distinct environmental and structural features of biomolecular condensates, Nat. Phys. 21, 778 (2025).
- [105] A. Sharma, A. Sau, S. Dave, S. Roychowdhury, S. Schnorrenberg, R. Chowdhury, S. Hutten, D. Dormann, and S. M. Musser, Clustering within a single-component biomolecular condensate, bioRxiv, https://doi.org/10.1101/2025.08.18.670948.
- [106] A. V. Weigel, M. M. Tamkun, and D. Krapf, Quantifying the dynamic interactions between a clathrin-coated pit and cargo molecules, Proc. Natl. Acad. Sci. USA 110, E4591 (2013).
- [107] C. Manzo, J. A. Torreno-Pina, P. Massignan, G. J. Lapeyre, M. Lewenstein, and M. F. Garcia Parajo, Weak ergodicity breaking of receptor motion in living cells stemming from random diffusivity, Phys. Rev. X 5, 011021 (2015).
- [108] F. Nakai and T. Uneyama, Brownian yet non-Gaussian diffusion of a light particle in heavy gas: Lorentz-gas-based analysis, Phys. Rev. E 108, 044129 (2023).
- [109] K. Sakamoto, T. Akimoto, M. Muramatsu, M. S. P. Sansom, R. Metzler, and E. Yamamoto, Heterogeneous biological membranes regulate protein partitioning via fluctuating diffusivity, PNAS Nexus 2, pgad258 (2023).